Science and Technology Indonesia
e-ISSN:2580-4391 *p*-ISSN:2580-4405
Vol. 10, No. 2, April 2025

Research Paper

A Small Amount of Sn Addition Effect to Cu-15Zn Alloy on Structure, Microstructure, Hardness, Corrosion Resistance, and Antibacterial Activity

Imam Basori[1*], Yunita Sari[1], Dendy Wardhana Prasetya[1], Ferry Budhi Susetyo[1], Juliawati Alias[2], Setia Budi[3], Sigit Dwi Yudanto[4], Muhammad Yunan Hasbi[4], Evi Ulina Margareta Situmorang[5], Daniel Edbert[6]

[1]*Department of Mechanical Engineering, Universitas Negeri Jakarta, Jakarta Timur, 13220, Indonesia*
[2]*Faculty of Mechanical and Automotive Engineering Technology, Universiti Malaysia Pahang Al-Sultan Abdullah, Kuantan, 26300, Malaysia*
[3]*Department of Chemistry, Universitas Negeri Jakarta, Jakarta Timur, 13220, Indonesia*
[4]*Research Center for Metallurgy, National Research and Innovation Agency, KST BJ Habibie South Tangerang, Banten, 15314, Indonesia*
[5]*Department of Physiology School of Medicine and Health Sciences, Atma Jaya Catholic University of Indonesia, Jakarta, 14440, Indonesia*
[6]*Department of Microbiology School of Medicine and Health Sciences, Atma Jaya Catholic University of Indonesia, Jakarta, 14440, Indonesia*
*__Corresponding author__: imam-basori@unj.ac.id

Abstract
CuZn alloy is widely used as a heat exchanger pipe and also for cardiovascular implant applications. Several problems have been found in that alloy, such as less corrosion resistance. Therefore, various Sn (0.2, 0.7, 1, and 2 wt.%) were added to Cu-15Zn alloy in the present research to enhance corrosion resistance. Afterwards, the alloy was homogenized at 800 °C for 2 hours. Several investigations were conducted, such as structure, microstructure, hardness, corrosion resistance, bacterial activity, and thermal analysis using XRD, optical microscope, Vickers hardness, potentiostat, digital camera, and thermogravimetric analyzer, respectively. More Sn content leads to an increase in volume and a decrease in hardness. Presenting Sn in the alloy does not influence the phase in the alloy microstructure. The highest Sn content in the alloy promoted a more positive value of the alloy, indicating that the sample is more cathodic, probably due to the protective layer on the surface. A concentration of 1 wt.% Sn exhibits the most effective antibacterial effect probably due to the small crystallite size. Shifting to a higher temperature increased the samples weight, indicating oxides formed on the samples surface.

Keywords
Brass, XRD, Optical Microscope, Vickers Hardness, Potentiostat

Received: 2 October 2024, Accepted: 3 February 2025
https://doi.org/10.26554/sti.2025.10.2.443-451

1. INTRODUCTION

CuZn alloy, known as brass, has superior properties such as thermal conductivities, corrosion resistance, antibacterial properties, and better hardness than pure Cu (Basori et al., 2024; Bhaskar and Jagirdar, 2017; Marichamy et al., 2016). Comparing to the CuAl, CuZn has better shape memory capacities and more ductile (Alaneme and Okotete, 2016). CuZn alloys also have better tensile strength than Mg-RE-based alloys, Mg-6Zn and Zn1Mg,Ca,Sr (Tang et al., 2017). Moreover, CuZn alloy could maintain the porous 3D structure much better than Zn (Varzi et al., 2018).

Many applications use CuZn nowadays, such as screws, wire, heat exchanger pipes, and capacitors (Achiţei et al., 2017). Moreover, Tang et al. (2017) developed CuZn alloys as a cardiovascular implant application. Several problems have been found in brass alloy, such as less corrosion resistance. Furthermore, heat exchanger pipes commonly use HCl for sludge cleaning (Ashmawy et al., 2022). Therefore, some researchers enhanced corrosion resistance by adding an element, heat treatment, or coating to that alloy. Adding elements to brass is more straightforward than other methods because it can be conducted during casting, making it more efficient and less costly.

Mn, Pb, Al, and Sn are commonly added to CuZn alloy for different purposes. Hendrawan et al. (2021) added 9 wt.% of Mn to Cu-31Zn using casting for enhanced hardness. Johansson et al. (2022) have stated that Pb was added to increase the machinability of the brass alloy. Alam et al. (2021) have added various Al (2, 4, and 6 %) to the brass alloy to increase the hardness and tensile strength. Shamaki et al. (2023) added various concentrations of Sn (0.5 to 4 wt.%) to Zn-4Cu and aged several times to investigate the morphology, crystallographic orientation, and hardness behavior. Altaf et al. (2019)

investigate the corrosion behavior of Cu, CuZnMn, CuZnPb, CuZnSn, and CuZnAl, resulting in the corrosion rates of 0.132, 0.019, 0.014, 0.010, and 0.009 mmpy, respectively.

Pb is a toxic material; therefore, Moustafa et al. (2016) have investigated by replacing Pb with Sn in a CuZn alloy. Sn-brass improves machinability rather than Pb-brass. Moreover, adding Sn into CuZn could also enhance hardness. Kenevisi and Nasab added Sn around 4.82 wt.% into the Cu-35 Zn, successfully enhancing corrosion resistance in a 3.5 % NaCl solution (Kenevisi and Nasab, 2014). Chuaiphan et al. (2013) added 1% Sn into $Cu_{40}Zn$ alloy and found $\alpha + \beta$ duplex phase in the alloy with and without Sn addition. Therefore, it can be concluded that 1% Sn did not influence the microstructure change. Furthermore, Rajabi and Doostmohammadi (2018) developed $Cu_{30}Zn_xSn$ alloys (x=1.2, 3.2. 5.4, 8, 11.4. 13.7 and 17.4%) and the resulting higher Sn content (>1.2) led to increased hardness due to the microstructure formed duplex (α+β') and (β'+γ) brass.

The antimicrobial effects of oligodynamic metals may differ from the concentration gradients of common antimicrobial agents. The balance of redox potentials and the formation of hydroxyl radicals play a significant part in the antibacterial mechanism of oligodynamic metals. Sn has also been reported to be Rajabi a catalyst in the oxidation process, esterification, and the synthesis of organic compounds (Didenko et al., 2018; Kim et al., 2023; Villapún et al., 2016). The contribution of Sn as a catalyst explains that a specific concentration of the metal is needed to be highly effective in supporting the oligodynamic effects of Cu and Zn. Various Sn was also added to the alloy to enhance the oligodynamic effect. Jan et al. (2013) study found that doped Sn in the 4% ZnO successfully enhanced the inhibition zone from 14 to 22 mm of *Staphylococcus aureus* bacteria. Selvinsimpson et al. (2021) added 5% of Sn into ZnO, increasing the inhibition zone from 6 to 14 mm of *S. typhi* bacteria. Kang et al. (2016) study found the antibacterial (*Staphylococcus aureus*) efficiency of Si and CuSn-53 are 0%, while CuSn-63 and CuSn-83 are 99.4 and 100%, respectively.

It seems that CuZnSn alloy promises superior properties, especially for enhanced corrosion resistance. Therefore, in the present research, various Sn (0.2, 0.7, 1, and 2 wt.%) were added to the Cu-15Zn alloy to enhance corrosion resistance. Afterward, the alloy was homogenized at 800 °C for 2 hours. The primary investigation uses potentiostat equipment to examine corrosion phenomena in 0.1 M HCl. In addition, several investigations were conducted, such as structure, microstructure, hardness, antibacterial activity, and thermal analysis, using XRD, optical microscope, Vickers hardness, digital camera, and thermogravimetric analyzer.

2. EXPERIMENTAL SECTION

2.1 Materials

The commercial rods were used in this experiment to make the alloys. Cu, Zn, and Sn have purities of 99.98, 99, and 99.94 wt.% respectively.

2.2 Instrumentation

A customized electrical furnace was used to melt the materials. Several instrumentations were used for material characterization. XRD was conducted using Bruker D8 Advance 3kW with LynxEye XE-T detector and Cu Kα radiation. The Olympus GX71-N453U optical microscope was used to investigate the microstructure. The Future-Tech FV-300e Vickers hardness tester was used to investigate the hardness. Edag ER466 Potentiostat equipment was used to investigate corrosion behavior. The antibacterial activity results of the present study were documented using a digital camera (Samsung S22 Galaxy). Thermal analysis was determined using NETZSCH TG 209 F3 Tarsus apparatus.

2.3 Procedure

Cu was inserted into the crucible and melted in the electric furnace at 1200 °C temperature. After the Cu melted, the crucible was taken out from the furnace, and a Zn rod was added to the crucible and then stirred manually. Mixed Cu and Zn were then heated in an electric furnace at 1150 °C. Afterwards, the mixed Cu and Zn were taken out, and various Sn (0.2, 0.7, 1, and 2 wt.%) were added separately, manually stirred, and cast in the mold (110×110×6 mm). Before the melted alloy was poured, the mold was heated to 700 °C. All as-cast alloy ingots were homogenized at an 800 °C temperature for 2 hours and then cooled using natural air cooling (Basori et al., 2018). The composition of various alloys can be seen in Table 1.

2.4 Characterization

XRD measurement was scanned from 30 to 100° (step size 0.02°) and then XRD patterns were refined using GSAS software. Moreover, the sample was cut (10×10×6 mm) and mounted in epoxy resin. It was polished using abrasive paper (200 up to 2000), polished with alumina (0.3 μm), and rinsed with water. Afterward, the sample was etched using a $FeCl_3$ solution (5 g $FeCl_3$ + 50 mL alcohol) for 3 seconds, then rose using alcohol and dried using an electric dryer. The optical microscope was used to investigate the microstructure of the etching sample.

The mounted sample using epoxy resin was polished using abrasive paper (200 up to 2000) for hardness measurement. The Vickers hardness tester was used to investigate the hardness value using 1 kg of load. Five spot measurements were taken on top of the polished samples.

Potentiostat equipment was used to investigate corrosion behavior in 0.1 M HCl. Ag/AgCl is the reference electrode, platinum wire is the counter electrode, and the alloy sample is the working electrode. Corrosion behavior investigation was recorded from -250 to +800 mV using a scan rate of 1 mV/s. Moreover, the Tafel extrapolation method was used to determine corrosion potential and current density. The corrosion rate will be found using the following expression (Ahmad, 2006).

Table 1. Compositions of Various Cuznsn Alloys

Sample	Composition (wt.%)				
	Cu	Zn	Sn	Co	Bi
Cu-15Zn-0.2Sn	Balance	15.1	0.180	0.033	0.288
Cu-15Zn-0.7Sn	Balance	15	0.735	0.029	0.279
Cu-15Zn-1Sn	Balance	15.8	0.948	0.035	0.293
Cu-15Zn-2Sn	Balance	14.5	2.01	0.027	0.285

$$\text{Corrosion rate (mmpy)} = C\frac{M \times icorr}{n \times \rho} \quad (1)$$

Where C is the constant (3.27), M is the atomic weight (g/mol), icorr is the corrosion current density (A/cm^2), n is the number of electrons, and ρ the density (g/cm^3). The antibacterial activity procedure is explained in the following paragraph. The experiment result was documented using a digital camera.

2.4.1 Sterility Test

The samples were submerged in 10 mL sterile distilled water inside 50 mL centrifuge tubes for 30 minutes and then put into a vortex for 30 seconds. 1 mL of the water is inoculated on a Trypticase Soya agar plate + 5 % Sheep Blood and then incubated at 35 °C for 24 hours. Before testing, the samples were let air dry and swabbed with 70 % ethanol.

2.4.2 Direct Contact Assay and Diffusible Metal Observation

Staphylococcus aureus ATCC 25923 was used in this test. A suspension of 0.5 Mc Farland was poured onto the surface of Mueller Hinton Agar. Each plate was swabbed 3 times with a rotation of 60° to ensure the plate was covered with the suspension. The materials were placed on the Mueller-Hinton Agar plate. The inoculated plates were incubated at 35 ±2 °C for 24 hours, and then the inhibition zone was assessed using the unaided eye. Moreover, diffusible metal was observed using an unaided eye, and any changes inside the agar plate were documented.

2.4.3 Regrowth Assessment

After incubation, the materials were removed using sterile forceps. The agar is re-incubated at 35±2 °C for another 24 hours to observe the antimicrobial activity post-contact.

2.4.4 Fluid Contact Assay

Staphylococcus aureus ATCC 6538P was used in this test. The test materials were placed in a petri dish filled with a 10 mL suspension of the test microorganism with turbidity equal to 105 CFU/mL. Ten microliters of the suspension were shown every 1 hour for 8 hours to observe the reduction of the bacterial population in contact with the metal. The suspension was aspirated adjacent to the metal surfaces. The suspension was inoculated an MSA agar plate for each dilution using the drop plate method to ensure that only *Staphylococcus aureus* was present and to quantify the growth.

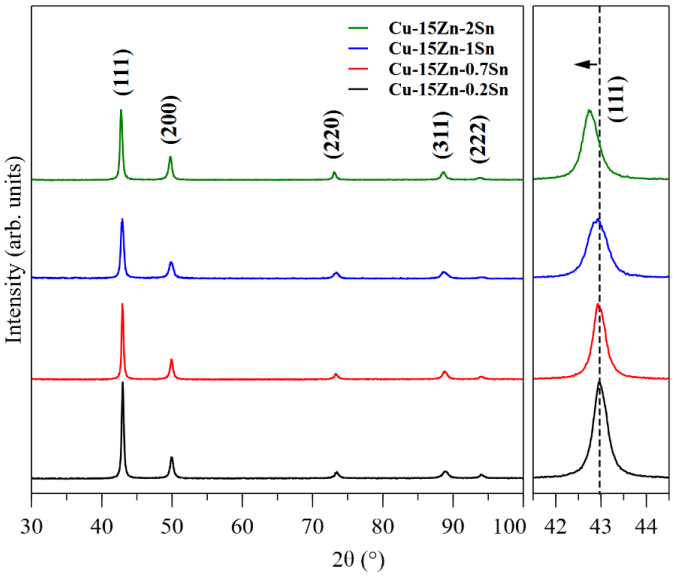

Figure 1. XRD Pattern of Various Alloys. The Right Image Shows the Magnification of the Diffraction Pattern 2θ = 41.5 – 44.5°

Thermal analysis was determined using Thermogravimetric analyzer apparatus. Thermal analysis was conducted to result in mass loss of the sample (3×3×3 mm) during heating with a temperature range from 200-1000 °C under a nitrogen environment.

3. RESULTS AND DISCUSSION

3.1 Structure

Cu-15Zn-0.2Sn, Cu-15Zn-0.7Sn, Cu-15Zn-1Sn, and Cu-15Zn-2Sn samples were investigated using Bruker D8 Advance 3kW with LynxEye XE-T detector and Cu Kα radiation. XRD was scanned from 30 to 100° (step size 0.02°). Afterward, XRD patterns were refined using GSAS software.

In Figure 1, we can see the diffraction patterns of Cu-Zn alloys with various Sn additions. It has been confirmed that the indexed peaks (111), (200), (220), (311), and (222) in the four diffraction patterns belong to the α-brass phase. Qualitatively, the face-centered cubic α-brass phase (Cu0.85Zn0.15) with space group fm-3m is in agreement with JCPDS No. 018-

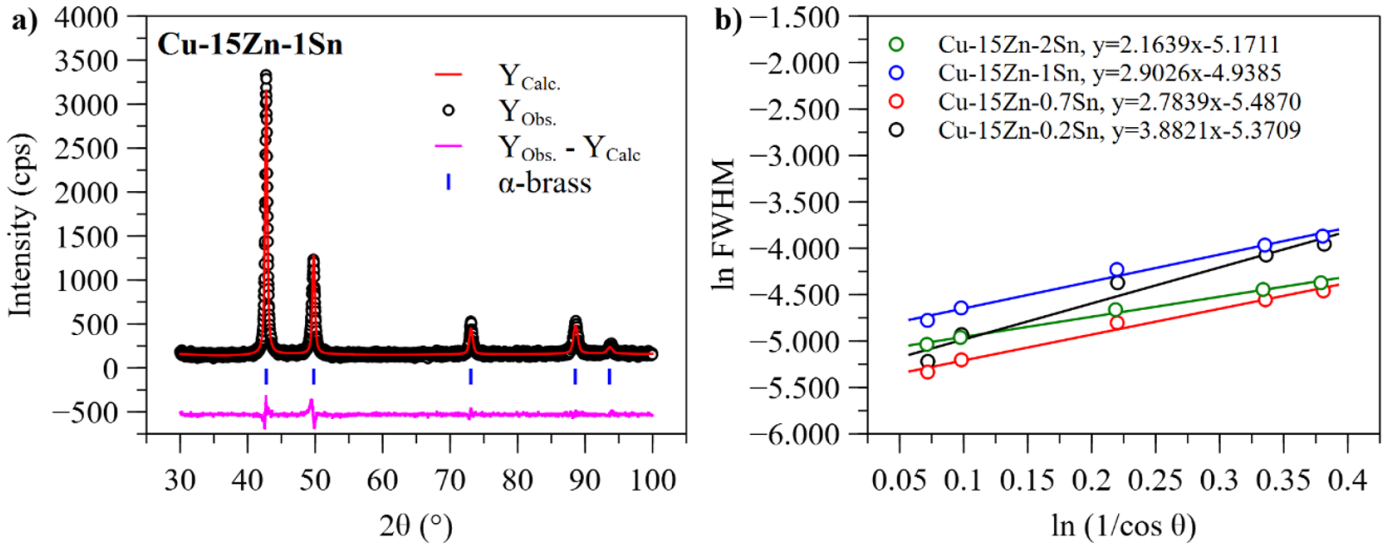

Figure 2. (a) Plot of Observed Diffraction Patterns vs. Calculated Using the Rietveld Method for Cu-15Zn-1Sn Sample, and (b) Plot in (1/cos θ) vs. ln FWHM. The Straight Line is the Result of Linear Regression of the Four Samples

5556. The single phase of α-brass matches the findings of other researchers (Babouri et al., 2019; Heidarzadeh et al., 2022).

With an increase in Sn concentration, there is a shift in the peak on the indexed plane (111), as observed by magnification of the diffraction pattern at 2θ = 41.5-44.5°. This implies that Sn addition will result in lattice disorder. In the sample with 1 wt.% Sn addition, peak broadening as well as peak shifting are seen. It would be interesting to conduct a quantitative analysis of the diffraction patterns of the four alloys. The Rietveld method was used to confirm the lattice constant of the α-brass phase crystal (Larson and Dreele, 2004). Figure 2 (a) compares the observed diffraction pattern to the calculation for the Cu-15Zn-1Sn sample. The calculation results show that the lattice constants a = b = c of the α-brass crystal increase from 3.6545 Å (Cu-15Zn-0.2Sn sample) to 3.6597 Å (Cu-15Zn-2Sn sample) as the Sn content of the Cu-15Zn alloy rises. Growth of the α-brass crystal volume is a subsequent effect.

Finally, the crystallite size of each alloy sample is estimated using the fitted diffraction pattern. The modified Scherrer method is used to estimate the crystallite size through the full width at half maximum (FWHM) value of each peak in the calculated diffraction pattern (Monshi et al., 2012; Syamsuir et al., 2023). The modified Scherrer approach is based on the construction of a straight-line equation between ln FWHM and ln (1/cos θ). Figure 2 (b) illustrates the straight-line relationship between ln (1cos θ) and ln FWHM. The crystallite size estimation calculation indicates that the Cu-15Zn-1Sn sample with the broadest peak at the indexed plane (111) has the smallest crystallite size of 202 Å. Table 2 lists the findings of the calculation of the lattice constant and crystallite size for each of the four samples.

3.2 Microstructure

Cu-15Zn-0.2Sn, Cu-15Zn-0.7Sn, Cu-15Zn-1Sn, and Cu-15Zn-2Sn samples surface morphology were captured using Olympus GX71-N453U optical microscope. Prior to surface morphology capture, the sample was cut (10×10×6 mm) and mounted in epoxy resin. It was polished using abrasive paper (200 up to 2000), polished with alumina (0.3 μm), and rinsed with water. Afterward, the sample was etched using $FeCl_3$ solution (5 g $FeCl_3$ + 50 mL alcohol) for 3 seconds, then rinsed using alcohol and dried using an electric dryer.

Figure 3 (a-d) presents the microstructure of CuZnSn alloys. Optical microscopy reveals that all alloys exhibit a consistent single α-phase, regardless of the Sn content. This corresponds to the diffraction pattern shown in Figure 1. The addition of Sn does not appear to have a significant impact on the morphology of the alloys, with the grain size remaining relatively unchanged across all samples. This consistency in grain size and phase structure indicates that Sn is fully dissolved within the α-matrix, suggesting effective alloying (Shamaki et al., 2023). Additionally, annealing twins observed in the α-fcc matrix, particularly in the sample with 0.7 wt.% Sn as shown in Figure 3 (b), are attributed to the low stacking fault energy of the alloy (Al-Fadhalah et al., 2021). These twins, formed during the annealing process, further highlight its intrinsic properties. Overall, the results suggest that the introduction of Sn into the CuZn matrix does not lead to significant morphological changes, with the α-phase remaining stable and the grain structure largely unaffected by variations in Sn concentration.

3.3 Hardness

Cu-15Zn-0.2Sn, Cu-15Zn-0.7Sn, Cu-15Zn-1Sn, and Cu-15Zn-2Sn samples average hardness was determined using the Future-Tech FV-300e Vickers hardness tester (1 kg of load).

Table 2. Crystallography Data From Diffraction Patterns of Various Alloys

Source	Cu-15Zn-0.2Sn	Cu-15Zn-0.7Sn	Cu-15Zn-1Sn	Cu-15Zn-2Sn
α-brass phase	System crystal: Face-centered cubic (fcc) Space group: Fm-3m Space group number: 225			
Lattice constants a=b=c (Å)	3.6545	3.6567	3.6575	3.6597
Volume (Å^3)	48.807	48.896	48.927	49.015
wRp (%)	8.26	9.46	7.64	8.61
Rp (%)	6.21	7.21	5.90	6.66
GoF	1.638	1.756	1.499	1.494
Crystallite size (Å)	311	350	202	255

Table 3. Corrosion Properties of the Alloys

Alloy type	Corrosion potential (V) vs Ag/AgCl	Corrosion current density (A/cm^2)	Corrosion rate (mmpy)
Cu-15Zn-0.2Sn	-0.107	5.156×10^{-6}	4.41
Cu-15Zn-0.7Sn	-0.117	5.271×10^{-6}	4.512
Cu-15Zn-1Sn	-0.109	4.977×10^{-6}	4.264
Cu-15Zn-2Sn	-0.092	4.821×10^{-6}	4.134

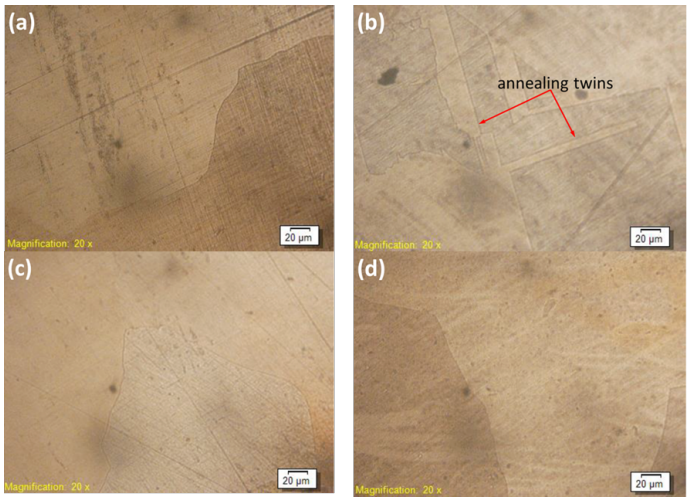

Figure 3. Microstructure of the Various Alloys(a) Cu-15Zn-0.2Sn, (b) Cu-15Zn-0.7Sn, (c) Cu-15Zn-1Sn, and (d) Cu-15Zn-2Sn

Five spot measurements were taken on top of the polished samples. Prior the hardness measurement, the mounted sample was polished using abrasive paper (200 up to 2000).

The average hardness of various alloys can be seen in Figure 4. Shahriyari et al. found Cu-15Zn hardness is 66 VHN due to annealing at 0.8 of their melting temperature (Shahriyari et al., 2022). While, Ezequiel et al. have found that Cu-15Zn (as-received) has a hardness of 75 HV (Ezequiel et al., 2024). Therefore, it can be concluded that the hardness of Cu-15Zn depends on the treatment conditions. Compared to the Cu-15Zn-0.2Sn sample, presenting a 0.2 wt.% of Sn could enhance the hardness of the alloy. According to Figure 4, it can be seen that an increase in Sn content led to a decrease in hardness, which perfectly agrees with another study (Si, 2018). Higher hardness is seen in the Cu-15Zn-0.2Sn sample, while lower hardness is seen in the Cu-15Zn-2Sn sample. Adding Sn depends on Sn softening; therefore, it could decrease hardness with increased Sn content in the alloy (Si, 2018).

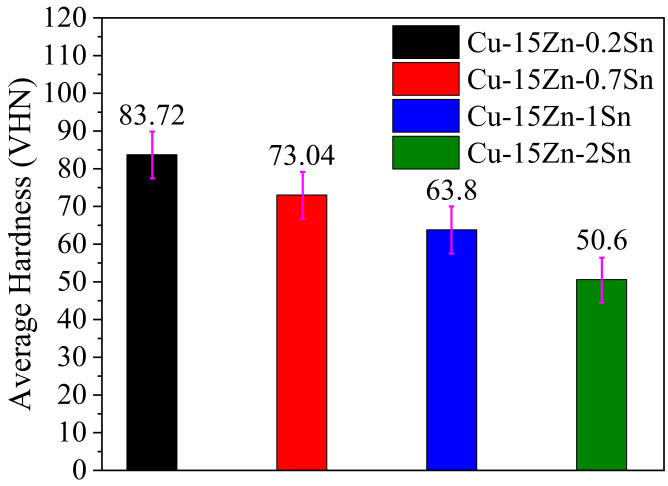

Figure 4. Average Hardness of the Alloy

3.4 Corrosion Resistance

Cu-15Zn-0.2Sn, Cu-15Zn-0.7Sn, Cu-15Zn-1Sn, and Cu-15Zn-2Sn samples corrosion measurements were determined using Edag ER466 Potentiostat equipment in 0.1 M HCl. Corrosion behavior investigation was recorded from -250 to +800

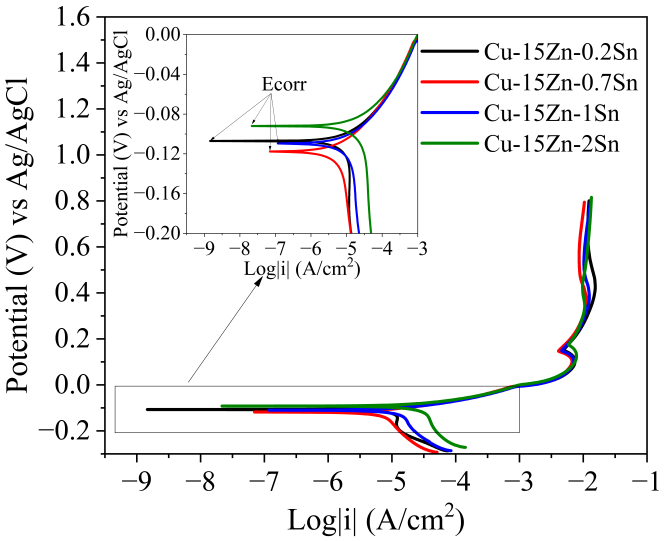

Figure 5. Potentiodynamic Polarization Curve of the alloys

mV using a scan rate of 1 mV/s. The corrosion measurement results of various alloys can be seen in Figure 5. Moreover, using the Tafel extrapolation method from Figure 5, corrosion potential and current can be found. Corrosion rate can be found by using Equation (1). Corrosion potential, corrosion current, and corrosion rate are summarized in Table 3.

Based on Table 3, it can be seen that the highest Sn content in the alloy promoted a more positive value of the alloy, which indicates the sample is more cathodic, probably due to the protective layer being formed on the surface. According to Kenevisi and Nasab study, presenting a Sn in the alloy could inhibit the dezincification of the CuZn by forming a protective layer on the surface (Kenevisi and Nasab, 2014). This condition could imply less corrosion current in the sample. In contrast, Cu-15Zn-0.7Sn has a more negative value than other samples, which indicates that the sample is more anodic, probably due to the dissolution of the sample surface in the solution. This condition would influence the rise in the corrosion current. Lv et al. (2022) have stated that the corrosion potential value represents the possibility of corrosion. A rise in corrosion potential could increase the possibility of increasing corrosion. Moreover, the corrosion current directly influences the corrosion rate. The more corrosion current is the more corrosion rate.

Another factor that could influence the corrosion current is the concentration of the solution. Wu et al. (2024) have investigated brass H57 in 0.1M HCl and found a corrosion current of 5.73 μA/cm^2. Moreover, Ashmawy et al. (2022) investigated brass in 1M HCl and found a corrosion current of 259± 5.1 μA/cm^2. Therefore, it can be concluded that the concentration of the HCl medium also influences the corrosion current. A rise in concentrations leads to an increase in the corrosion current.

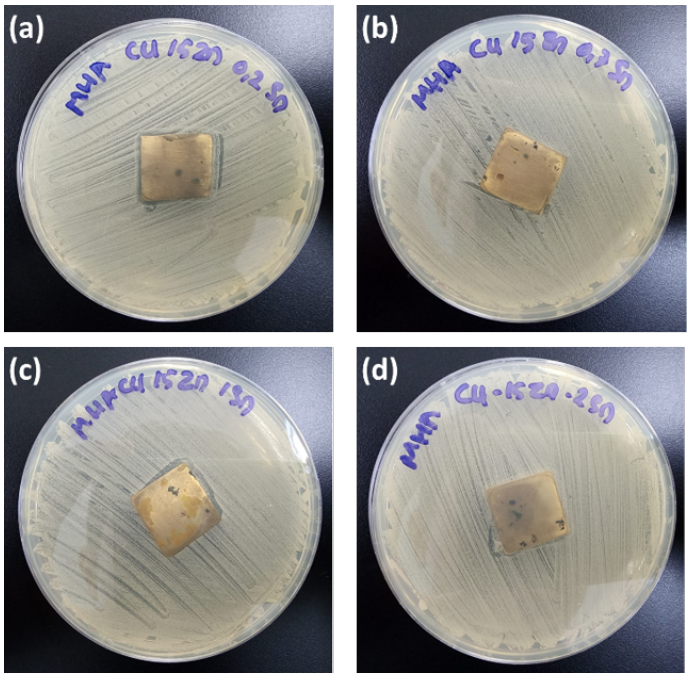

Figure 6. Direct Contact Test of the Materials (a) Cu-15Zn-0.2Sn, (b) Cu-15Zn-0.7Sn, (c) Cu-15Zn-1Sn, and (d) Cu-15Zn-2Sn

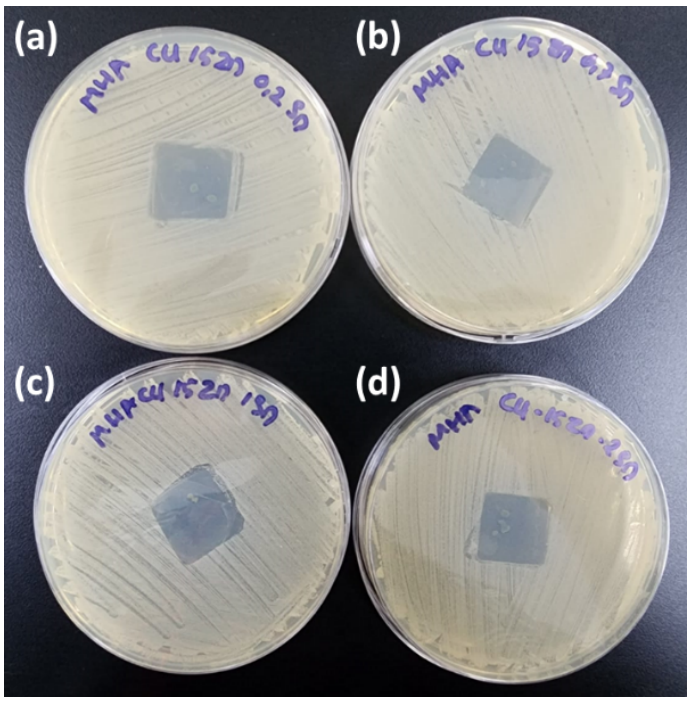

Figure 7. 24 Hours Post Contact Observation of the Various Alloys (a) Cu-15Zn-0.2Sn, (b) Cu-15Zn-0.7Sn, (c) Cu-15Zn-1Sn, and (d) Cu-15Zn-2Sn

3.5 Antibacterial Activity

Cu-15Zn-0.2Sn, Cu-15Zn-0.7Sn, Cu-15Zn-1Sn, and Cu-15Zn-2Sn antibacterial activity were determined using a digital

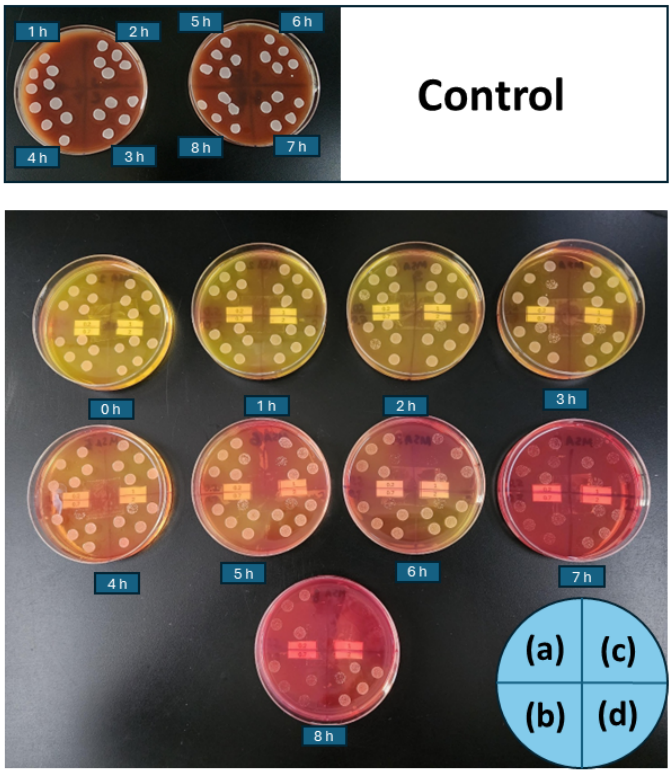

Figure 8. Fluid Contact Assay Measurement By Drop Plate Method (a) Cu-15Zn-0.2Sn, (b) Cu-15Zn-0.7Sn, (c) Cu-15Zn-1Sn, and (d) Cu-15Zn-2Sn

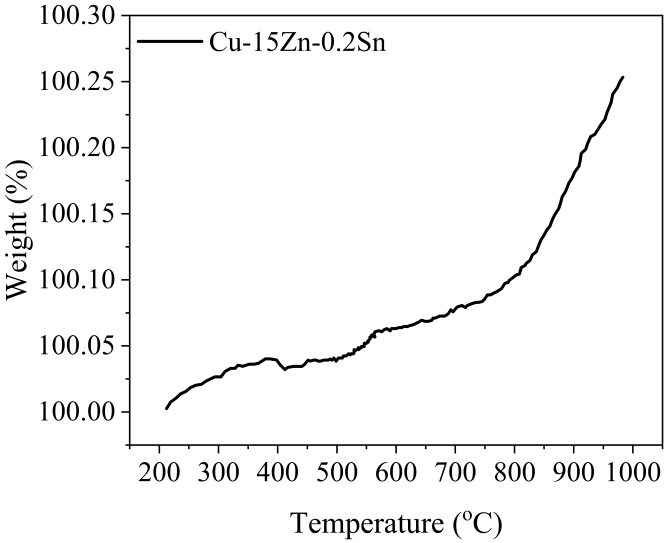

Figure 9. Thermal Analysis Result for Cu-15Zn-0.2Sn Sample

camera. Several step procedures were conducted, such as sterility tests, direct contact assay and diffusible metal observations, regrowth assessments, and fluid contact assays (detailed in the characterization section). *Staphylococcus aureus* was chosen as the model for the antibacterial effects of the alloy as it fits JIS Z2801, ISO 22196, and US EPA standards of standard microorganisms for antibacterial surfaces and products (Villapún et al., 2016). *Staphylococcus aureus* could affect skin disease, which is hard to treat with common antibiotics. Moreover, this bacteria could contaminate hospital implants, spread, and cause serious infections (Jan et al., 2013).

According to Figure 6, there was no growth under the metal or metallic material diffusion under the colony. This phenomenon is probably caused by previous heat treatment towards the alloy, limiting the ability of the metals to diffuse, but this does not limit the antibacterial activity of the metal. Moreover, the duration of contact between the Cu metal and *Staphylococcus aureus* is one of the main factors of the antibacterial activity besides the temperature and humidity of the contact (O'gorman and Humphreys, 2012).

Even though the metal is non-diffusible, the antibacterial effects remained effective in a contact mechanism as seen in Figure 7. There was no regrowth of the microorganism after removing the materials (24 hours post-contact observation); this showed the bactericidal mechanism of the metal. In this study, the antibacterial effects are solely caused by the presence of Cu and Zn metals (Yasuyuki et al., 2010). The presence of Cu and Zn ions appears to disturb the bacteria in multiple simultaneous ways, preventing the development of bacterial resistance and regrowth of the microorganism. The disruption of bacterial membrane integrity by contact with Cu surfaces. Cu ions have the ability to directly denature bacterial proteins, and through a Fenton-like chemistry, they can also cause the formation of highly damaging hydroxyl radicals, disrupting DNA, enzymes, and other proteins, as well as through the peroxidation of lipids and subsequent membrane damage (Villapún et al., 2016).

Fluid contact assay measurement by the drop plate method is seen in Figure 8. Two first blood agar plates are growth control plates. Colony reduction is observed after 7 hours of exposure. The most significant reduction is shown by Cu-15Zn-1Sn, in which total annihilation is reached within 8 hours of exposure. Overall, colony reduction as a function of time, which has perfect in agreement with another report (Kang et al., 2016). Moreover, the most effective antibacterial effect is exhibited by a concentration of 1 wt.% Sn probably due to the small crystallite size. According to the XRD investigation, Cu-15Zn-1Sn has the smallest crystallite size. Various researchers have reported that the smallest crystallite size increases antibacterial effects (Azam et al., 2012; Syamsuir et al., 2023).

3.6 TGA

Cu-15Zn-0.2Sn and Cu-15Zn-0.7Sn samples were determined using NETZSCH TG 209 F3 Tarsus apparatus. A thermal analysis investigation was conducted at a temperature range from 200 – 1000 °C under a nitrogen environment.

Figure 9 shows thermal analysis results for the Cu-15Zn-0.2Sn sample. Shifting to a higher temperature increased the sample's weight, indicating oxides formed on the sample's surface (Xu et al., 2022). Nyong et al. (2022) have found more

immersion time of the CuZn alloy at 650 °C leads to increased oxide thicknesses. Moreover, an extreme increment is seen when the temperature reaches 800 °C, which indicates more oxides are formed. Lejda et al. (2024) have found similar behavior at temperatures between 460 and 700 °C. According to Shi et al. (2014), the oxidation of the brass is relatively slow at lower temperatures, while it is more raised at higher temperatures.

4. CONCLUSIONS

Fabrication of the brass alloy has been successfully done using the casting method. More Sn content leads to an increase in volume and a decrease in the hardness of the brass alloy. The introduction of Sn into the CuZn matrix does not lead to significant morphological changes, with the α-phase remaining stable and the grain structure largely unaffected by variations in Sn concentration. An increase in Sn contents leads to increased corrosion resistance and a decrease in hardness. Higher Sn content led to a more positive value of the alloy, which indicates that the sample is more cathodic. Probably due to the protective layer being formed on the surface, it implies less corrosion current. The most significant colony reduction is shown by Cu-15Zn-1Sn, in which a total annihilation is reached within 8 hours of exposure, probably due to the small crystallite size. Moreover, shifting to a higher temperature increased the sample's weight, indicating oxides formed on the sample's surface.

5. ACKNOWLEDGEMENT

This research has been funded by the Faculty of Engineering Universitas Negeri Jakarta Collaboration Grant in 2024.

REFERENCES

Achiţei, D., P. Vizureanu, M. G. Minciună, N. Cimpoeşu, and B. Istrate (2017). Improvement of Structural Characteristics for Cuzn Alloy through Heat Treatments. *Key Engineering Materials*, **750**; 3–8

Ahmad, Z. (2006). *Principles of Corrosion Engineering and Corrosion Control*. Butterworth-Heinemann, Oxford, United Kingdom, 1st edition

Al-Fadhalah, K. J., M. A. Rafeeq, and N. Thomas (2021). Microstructure and Texture Development in Thermomechanically Processed Leaded Brass. *Metals*, **11**(7); 998

Alam, M. A., H. H. Ya, A. Ahmad, M. Yusuf, M. Azeem, and F. Masood (2021). Influence of Aluminum Addition on the Mechanical Properties of Brass/Al Composites Fabricated by Stir Casting. *Materials Today: Proceedings*, **48**; 811–814

Alaneme, K. K. and E. A. Okotete (2016). Reconciling Viability and Cost-Effective Shape Memory Alloy Options–A Review of Copper and Iron Based Shape Memory Metallic Systems. *Engineering Science and Technology, an International Journal*, **19**(3); 1582–1592

Altaf, F., R. Qureshi, A. Yaqub, and S. Ahmed (2019). Electrochemistry of Corrosion Mitigation of Brasses by Azoles in Basic Medium. *Chemical Papers*, **73**(5); 1221–1235

Ashmawy, A. M., R. Said, I. A. Naguib, B. Yao, and M. A. Bedair (2022). Anticorrosion Study for Brass Alloys in Heat Exchangers During Acid Cleaning Using Novel Gemini Surfactants Based on Benzalkonium Tetrafluoroborate. *ACS Omega*, **7**(21); 17849 –17860

Azam, A., A. S. Ahmed, M. Oves, M. S. Khan, and A. Memic (2012). Size-Dependent Antimicrobial Properties of CuO Nanoparticles Against Gram-Positive and -Negative Bacterial Strains. *International Journal of Nanomedicine*, **7**; 3527–3535

Babouri, L., K. Belmokre, A. Kabir, A. Abdelouas, R. Khettabi, and Y. El Mendili (2019). Microstructure and Crystallographic Properties of $Cu_{77}Zn_{21}$ Alloy Under the Effect of Heat Treatment. *Materials at High Temperatures*, **36**(2); 165–172

Basori, I., I. Angela, D. Jendra, and B. T. Sofyan (2018). Deformation Characteristics and Texture Development of Biadded Cu-29Zn Alloys. *IOP Conference Series: Materials Science and Engineering*, **378**(1); 012015

Basori, I., N. B. Sinaga, M. S. Ponco, Y. Sari, and S. T. Dwiyati (2024). Investigation of Aluminum Addition on the Microstructure and Mechanical Properties of Cu-31Zn-0.1Mn-xAl Alloys. *AIP Conference Proceedings*, **3116**(1); 1–6

Bhaskar, S. P. and B. R. Jagirdar (2017). A Journey From Bulk Brass to Nanobrass: A Comprehensive Study Showing Structural Evolution of Various Cu/Zn Bimetallic Nanophases From the Vaporization of Brass. *Journal of Alloys and Compounds*, **694**; 581–595

Chuaiphan, W., L. Srijaroenpramong, and D. Pinpradub (2013). The Effect of Tin and Heat Treatment in Brass on Microstructure and Mechanical Properties for Solving the Cracking of Nut and Bolt. *Applied Mechanics and Materials*, **389**; 237–244

Didenko, L. P., T. V. Dorofeeva, L. A. Sementsova, P. E. Chizhov, E. I. Knerel'man, and G. I. Davydova (2018). The Dehydrogenation of Propane on Platinum–Tin Glass-Fiber Woven Catalysts. *Kinetics and Catalysis*, **59**(4); 472–480

Ezequiel, M., I. Proriol Serre, T. Auger, E. Héripré, Z. Hadjem-Hamouche, and L. Perriere (2024). The Liquid Metal Embrittlement of a Reactive System at Room Temperature: α-Brasses in Contact With the Liquid Eutectic Ga-In. *Engineering Failure Analysispha*, **164**; 108694

Heidarzadeh, A., M. Javidani, and L. St-Georges (2022). Crystallographic Orientation Relationship Between α and β Phases During Non-Equilibrium Heat Treatment of Cu-37 Wt. % Zn Alloy. *Crystals*, **12**(1); 97

Hendrawan, C. N., A. Setyani, D. R. K. Pertiwi, and B. T. Sofyan (2021). Effect of 9 wt% Mn Addition on Cold Rolling and Annealing Behaviour of Cu-31Zn Alloy. *Materials Today: Proceedings*, **46**; 3346–3351

Jan, T., J. Iqbal, M. Ismail, M. Zakaullah, S. Haider Naqvi, and N. Badshah (2013). Sn Doping Induced Enhancement in the Activity of ZnO Nanostructures Against Antibiotic Resistant *S. Aureus* Bacteria. *International Journal of Nanomedicine*, **8**; 3679–3687

Johansson, J., P. Alm, R. M'Saoubi, P. Malmberg, J. E. Ståhl, and V. Bushlya (2022). On the Function of Lead (Pb) in Machining Brass Alloys. *International Journal of Advanced Manufacturing Technology*, **120**(11–12); 7263–7275

Kang, Y., J. Park, D. W. Kim, H. Kim, and Y. C. Kang (2016). Controlling the Antibacterial Activity of CuSn Thin Films by Varying the Contents of Sn. *Applied Surface Science*, **389**; 1012–1016

Kenevisi, M. S. and A. S. Nasab (2014). The Effect of Sn Addition and Sulfide Ion Concentration on the Corrosion Behavior of Cu-35Zn in NaCl Solution. *International Journal of Materials Research*, **105**(2); 188–193

Kim, B., M. T. Brueggemeyer, W. J. Transue, Y. Park, J. Cho, M. A. Siegler, and K. D. Karlin (2023). Fenton-Like Chemistry by a Copper(I) Complex and H_2O_2 Relevant to Enzyme Peroxygenase C−H Hydroxylation. *Journal of the American Chemical Society*, **145**(21); 11735–11744

Larson, A. C. and R. B. V. Dreele (2004). *General Structure Analysis System (GSAS)*, volume 748. University of California, Los Alamos

Lejda, K., J. Partyka, and J. F. Janik (2024). Thermogravimetric/Thermal–Mass Spectroscopy Insight Into Oxidation Propensity of Various Mechanochemically Made Kesterite Cu_2ZnSnS_4 Nanopowders. *Materials*, **17**(6); 1232

Lv, Y., X. Lang, Q. Zhang, W. Liu, and Y. Liu (2022). Study on Corrosion Behavior of (cuznmnni) 100- Xsnx High-Entropy Brass Alloy in 5 Wt% Nacl Solution. *Journal of Alloys and Compounds*, **921**; 166051

Marichamy, S., M. Saravanan, M. Ravichandran, and G. Veerappan (2016). Parametric Optimization of Electrical Discharge Machining Process on α–β Brass Using Grey Relational Analysis. *Journal of Materials Research*, **31**(16); 2531–2537

Monshi, A., M. R. Foroughi, M. R. Monshi, et al. (2012). Modified Scherrer Equation to Estimate More Accurately Nano-Crystallite Size Using Xrd. *World journal of nano science and engineering*, **2**(3); 154–160

Moustafa, M., I. Ahmed, M. Moustafa, and A. Ayoub (2016). Effect of Replacement of Lead by Tin on The Properties of Yellow Brass (Cu-Zn) alloy. *J. Basic Environ. Sci*, **3**; 107–111

Nyong, A. E., G. Udoh, J. J. Awaka-Ama, E. W. Nsi, and P. K. Rohatgi (2022). A Study of the Morphological Changes and the Growth Kinetics of the Oxides Formed by the High Temperature Oxidation of Cu-32.02% Zn-2.30% Pb Brass. *Materials Research*, **25**; e20210173

O'gorman, J. and H. Humphreys (2012). Application of Copper to Prevent and Control Infection. Where Are We Now? *Journal of Hospital Infection*, **81**(4); 217–223

Rajabi, Z. and H. Doostmohammadi (2018). Effect of Addition of Tin on the Microstructure and Machinability of α-Brass. *Materials Science and Technology*, **34**(10); 1218–1227

Selvinsimpson, S., P. Gnanamozhi, V. Pandiyan, M. Govindasamy, M. A. Habila, N. AlMasoud, and Y. Chen (2021). Synergetic Effect of Sn Doped Zno Nanoparticles Synthesized Via Ultrasonication Technique and Its Photocatalytic and Antibacterial Activity. *Environmental Research*, **197**; 111115

Shahriyari, F., M. H. Shaeri, A. Dashti, Z. Zarei, M. T. Noghani, J. H. Cho, and F. Djavanroodi (2022). Evolution of Mechanical Properties, Microstructure and Texture and of Various Brass Alloys Processed by Multi-Directional Forging. *Materials Science and Engineering: A*, **831**; 142149

Shamaki, A. E., H. Y. Zahran, and A. F. Abd El-Rehim (2023). Effect of Sn Addition on the Microstructure and Age-Hardening Response of a Zn-4Cu Alloy. *Crystals*, **13**(12); 1635

Shi, D., Q. Liu, Z. Zhu, J. Sun, and B. Wang (2014). Experimental Study of the Relationships Between the Spectral Emissivity of Brass and the Temperature in the Oxidizing Environment. *Infrared Physics and Technology*, **64**; 119–124

Si, Y. (2018). Research on Hardness and Tensile Properties of A390 Alloy With Tin Addition. In *IOP Conference Series: Materials Science and Engineering*, volume 322. page 022038

Syamsuir, F. B. Susetyo, B. Soegijono, S. D. Yudanto, Basori, M. K. Ajiriyanto, and C. Rosyidan (2023). Rotating-Magnetic-Field-Assisted Electrodeposition of Copper for Ambulance Medical Equipment. *Automotive Experiences*, **6**(2); 290–302

Tang, Z., J. Niu, H. Huang, H. Zhang, J. Pei, J. Ou, and G. Yuan (2017). Potential Biodegradable Zn-Cu Binary Alloys Developed for Cardiovascular Implant Applications. *Journal of the Mechanical Behavior of Biomedical Materials*, **72**; 182–191

Varzi, A., L. Mattarozzi, S. Cattarin, P. Guerriero, and S. Passerini (2018). 3D Porous Cu–Zn Alloys as Alternative Anode Materials for Li-Ion Batteries With Superior Low T Performance. *Advanced Energy Materials*, **8**(1); 1–11

Villapún, V. M., L. G. Dover, A. Cross, and S. González (2016). Antibacterial Metallic Touch Surfaces. *Materials*, **9**(9); 1–23

Wu, Z., H. Zhang, K. Feng, H. Yan, H. Song, C. Luo, and Z. Hu (2024). Consistency of In-Situ Brass Corrosion in HCl Solution Image Fluctuations and Electrochemical Potential Noise Revealed Through NARX Neural Network. *Journal of Materials Research and Technology*, **29**; 2279–2292

Xu, Y., K. Zhang, Z. Tian, R. Tong, K. Yu, and Y. Liu (2022). Comparison Research on Spectral Emissivity of Three Copper Alloys During Oxidation. *Infrared Physics and Technology*, **126**; 104344

Yasuyuki, M., K. Kunihiro, S. Kurissery, N. Kanavillil, Y. Sato, and Y. Kikuchi (2010). Antibacterial Properties of Nine Pure Metals: A Laboratory Study Using *Staphylococcus aureus* and *Escherichia coli*. *Biofouling*, **26**(7); 851–858